# EFFECTS OF INTER-ELM QUASI-COHERENT MODES ON THE DYNAMICS OF PEDESTAL TURBULENCE ON HL-2A TOKAMAK

J. Wen<sup>1</sup>, Z.B. Shi<sup>1\*</sup>, J.B. Wu, K.X. Han W.L. Zhong<sup>1</sup>, X.L. Zou<sup>2</sup>, M. Jiang<sup>1</sup>, R. Ke<sup>1</sup>, J.Q. Xu<sup>1</sup>, W. Chen<sup>1</sup>, Z.C. Yang<sup>1</sup>, A.S. Liang<sup>1</sup>, X. Yu<sup>1</sup>, N. Wu<sup>1</sup>, X.X. He<sup>1</sup>, P.W. Shi<sup>1</sup>, G.L. Xiao<sup>1</sup>, R.H. Tong<sup>1</sup>, Y.R. Zhu<sup>1</sup>, J.M. Gao<sup>1</sup>, M.K. Han<sup>1</sup>, Y. Shen<sup>1</sup> and X.Q. Ji<sup>1</sup>

1 Southwestern Institute of Physics, Chengdu 610041, China 2 CEA, IRFM, F-13108 Saint-Paul-Lez-Durance, France

3 Zhejiang University, Hangzhou 310027, China

Email: shizb@swip.ac.cn

Abstract: A study has been conducted on the effects of quasi-coherent modes (QCMs) on turbulence characteristics during edge-localized modes (ELMs) in HL-2A high-confinement mode (H-mode) discharges. These QCMs, predominantly electrostatic in nature, emerge between ELM events with frequencies around 40kHz with the frequency bandwidth of 20~50%. They are primarily confined to the pedestal region and are associated with the saturation of the density gradient. Observations reveal nonlinear interactions between QCMs and background turbulence, further supported by evidence of turbulence modulation in density due to radial electric field fluctuations from the modes. The presence of QCMs leads to an expansion in both radial and poloidal turbulence correlation lengths, influencing turbulent transport dynamics. Experimental findings indicate that QCMs substantially alter pedestal turbulence and transport by extending the correlation length and decorrelation time of turbulent structures. Additionally, the flow shearing rate in the pedestal is amplified to levels exceeding the turbulence decorrelation frequency. This enhanced shear flow stabilization suggests that QCMs may contribute to delaying ELM bursts by suppressing turbulence more effectively. These results highlight the critical role of QCMs in pedestal dynamics, demonstrating that their interplay with turbulence and shear flows governs pedestal stability and transport mechanisms.

Keywords: H-mode, pedestal, QCM, transport and confinement, plasma, tokamak

#### 1. Introduction

Plasma confinement in toroidal magnetic confinement configuration devices, such as tokamaks and stellarators, is often limited by cross-field transport processes, which lead to significant particle and energy losses. These transport mechanisms arise from various phenomena, including collisional diffusion, turbulence-driven mixing, convective cells, avalanches, and relaxation oscillations such as sawteeth and edge-localized modes (ELMs) [1–3]. While neoclassical transport—driven by Coulomb collisions in toroidal geometry—is always present [4], the dominant contributor to plasma losses is typically anomalous transport, which stems from microinstabilities and turbulence. This turbulent transport can exceed neoclassical levels by one to two orders of magnitude [5], degrading confinement and posing a major challenge for fusion reactor performance. Understanding and controlling these transport mechanisms is therefore critical for optimizing future fusion devices.

Significant progress has been made in improving plasma confinement through advanced operational regimes, such as the internal transport barrier (ITB) [6] and the high-confinement mode (H-mode) [7]. The H-mode regime is characterized by the formation of a transport barrier at the plasma edge, known as the pedestal, which may play a pivotal role in overall confinement by regulating edge dynamics and influencing core plasma conditions [8]. However, the steep pressure and density gradients in the pedestal also provide free energy that can drive micro-instabilities, including both electrostatic and electromagnetic fluctuations. While electromagnetic turbulence can be directly measured through magnetic probes, electrostatic fluctuations present a more complex challenge due to their strong nonlinear interactions with coherent structures such as zonal flows (in L-mode) and quasi-

1

coherent modes (QCMs) in H-mode. Although the role of zonal flows in turbulence regulation has been extensively studied, the interplay between QCMs and turbulence remains an open question, with important implications for H-mode confinement physics [9, 10].

Unlike well-defined linear instabilities, QCMs are not strictly characterized by a single physical mechanism but rather emerge from the nonlinear interaction between coherent modes and broadband turbulence in frequency space [11–17]. They typically exhibit spectral characteristics with a dominant peak frequency ( $f_{peak}$ ) and a broad frequency bandwidth ( $\Delta f$ ), with  $\Delta f/f_{peak}$  being several tens of percent [18]. These modes represent a hybrid between coherent and pure turbulent fluctuations, making their underlying physics essential for understanding pedestal transport dynamics.

QCMs have been observed across multiple tokamaks, attracting considerable research interest. On JET, broadband high-frequency oscillations—often termed "washboard modes"—have been detected in both carbon-wall and ITER-like wall discharges [19–20], with their modulation linked to divertor emission patterns [21]. Micro-tearing modes have been identified as a key driver of magnetic fluctuations in JET's pedestal, supported by nonlinear simulations matching experimental transport levels [22]. Similarly, DIII-D has reported high-frequency OCMs (80-250 kHz) in quiescent H-mode (OH-mode) plasmas, exhibiting characteristics consistent with kinetic ballooning modes (KBMs) [23]. These modes correlate with electron temperature pedestal saturation, limiting pressure gradients via enhanced transport [24]. Furthermore, nonlinear coupling between QCMs and pedestal distortions has been proposed as a mechanism for triggering ELMs relevant to future reactors [25]. On EAST, both electrostatic and electromagnetic OCMs have been documented [13], while HL-2A observations suggest that QCMs may arise from trapped electron modes (TEMs) driven by critical electron temperature gradients [11, 26]. Notably, QCMs have been associated with Type-III ELM dynamics [27] and, more recently, with the suppression of Type-I ELMs, potentially enabling extended ELM-free operation [7,28]. Advances in gyrokinetic and gyrofluid simulations [29] have bridged theory and experiment, though a complete understanding of QCM instabilities remains an open challenge requiring multiscale nonlinear analyses.

Given their impact on pedestal stability, QCMs and their interaction with turbulence are of paramount importance for ITER and future reactors. Turbulence in the pedestal exhibits a dual role: while excessive transport degrades confinement, moderate levels can help avoid dangerous pressure gradients that trigger ELMs [30]. However, the dynamics of QCMs are further complicated by sheared flows, which can suppress turbulence through decorrelation mechanisms [31]. The interplay between QCMs, turbulence, and flows remains poorly understood, necessitating further research to optimize confinement in high-performance plasmas.

This work investigates the influence of inter-ELM QCMs on pedestal turbulence in HL-2A. Section 2 describes the experimental setup and diagnostics, while Section 3 presents key findings on the nonlinear coupling between QCMs, turbulence, and flows. Conclusions and implications are discussed in Section 4.

## 2. Experimental arrangement

The HL-2A device is a medium-sized circular tokamak with a major radius of 165 cm, minor radius of 40 cm, and a closed divertor that can operate in either limiter or single-null (SN) divertor configurations [32]. It has achieved plasma currents of 480 kA, toroidal magnetic fields of 2.7 T, electron and ion temperatures of 5 keV and 4 keV respectively, and line-averaged densities of ~8×10<sup>19</sup> m<sup>-3</sup>. The carbon fiber composite (CFC)-lined vessel is

routinely siliconized to reduce wall recycling, and the device utilizes 2 MW NBI (45 keV), 3 MW ECRH (68 GHz), and 1 MW LHCD (3.7 GHz) for auxiliary heating and current drive. Recent experiments have demonstrated stable, repeatable ELMy H-mode plasmas under high-power heating, with ELM mitigation studies conducted using RMP, SMBI (1-6 ms pulses at 1.5-2 MPa), pellet injection, ECRH, and LHCD. For the present analysis, discharge conditions included  $B_t$ =1.2-1.4 T,  $I_p$ =150-180 kA, >1000 ms plateau durations, line averaged density  $n_{ea}$ =(2-5)×10<sup>19</sup> m<sup>-3</sup>,  $P_{NBI}$ =0.7-1 MW,  $P_{ECRH}$ =0.5-1.4 MW, and plasma stored energies of 20-30 kJ.

The experimental investigation of pedestal-region instabilities employed two primary diagnostic systems: Doppler backscattering reflectometry (DBS) [33,34] and beam emission spectroscopy (BES) [35]. The BES diagnostic utilizes a 32-channel two-dimensional detector array (as shown in Figure 1(a)) specifically configured for radial-poloidal turbulence correlation measurements. The system's observation window is optimized for the plasma boundary region, spanning radially from R=193 cm to R=203 cm with ~ 1 cm inter-channel spacing. Poloidally, the array configuration accommodates up to 4 detection channels with equivalent 1 cm spacing, providing comprehensive two-dimensional characterization. For microwave diagnostics, HL-2A features a multi-band DBS system covering Ka-band (26.5-40 GHz), Q-band (33-50 GHz), and V-band (50-75 GHz) frequencies. The pedestal measurement strategy combines O-mode and X-mode configurations: (1) an 8-channel X-mode system operating at 34-48 GHz (2 GHz step) probes the pedestal base to mid-pedestal regions, while (2) a 4-channel O-mode system at 31-37 GHz (2 GHz step) targets the pedestal top. Figure 1b illustrates the measurement coverage achieved through reflection cutoff layer analysis, with the combined systems providing complete high-resolution turbulence rotation profiles across both boundary and pedestal regions. The DBS systems operate with a nominal ~10° incidence angle, with exact measurement locations determined through ray-tracing analysis using density profiles obtained from frequency-modulated continuous wave (FMCW) reflectometry. While this introduces some positional uncertainty, the boundary-proximate measurement locations ensure minimal deviation (<10%) between estimated and actual measurement positions. This dual-diagnostic approach enables cross-validated measurements of key turbulence parameters including fluctuation spectra, correlation lengths, and rotation profiles throughout the pedestal region.

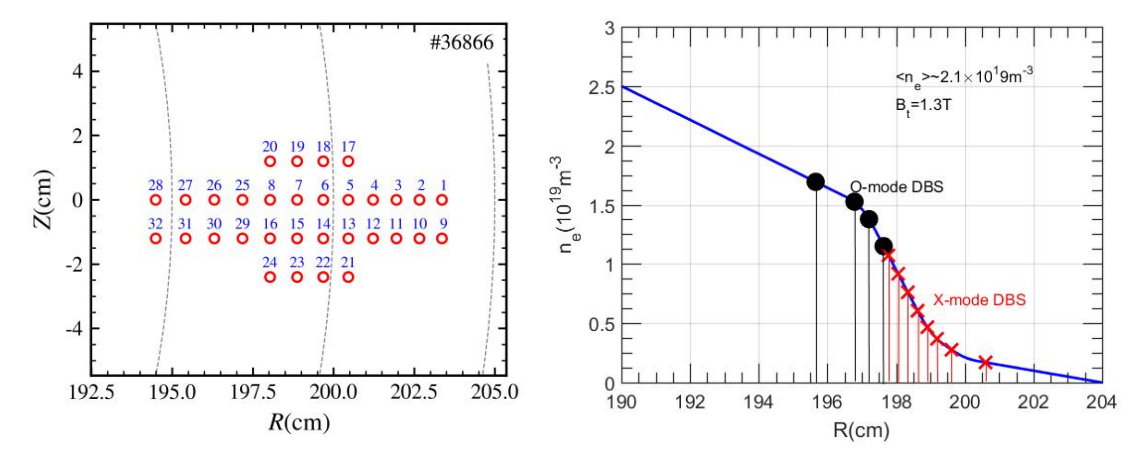


Figure 1. Measurement location of the BES and DBS systems

## 3. Characteristics of inter-ELM QCM at pedestal

Figure 2 presents the characteristic discharge evolution. Panel (a) displays the lineaveraged electron density measured by far-infrared (FIR) interferometry, while (b) shows the normalized beta (βN). Divertor Dα emission is plotted in (c), and (d)–(e) exhibit spectrograms of density fluctuations and magnetic signals, respectively. The pedestal density gradient ( $\nabla n_e$ ) is depicted in (f). The discharge employs neutral beam injection (NBI, PNBI = 0.7 MW) combined with 300 kW lower hybrid current drive (LHCD). H-mode transition occurs at ~845 ms following limit-cycle oscillations (initiated at 832 ms). As shown in Figure 2(d), a quasi-coherent mode (QCM) emerges in the 20-60 kHz range during the inter-ELM phase. Notably, QCM excitation consistently coincides with a critical pedestal  $\nabla n_e$  threshold (~2.5×10<sup>20</sup> m<sup>-4</sup> in these discharges). During QCM activity, the pedestal  $\nabla n_e$  continues to rise, while the mode's central frequency decays linearly from 60 kHz to 20 kHz—suggesting an inverse dependence on the gradient. This trend terminates when  $\nabla n_e$  exceeds ~3.8×10<sup>20</sup> m<sup>-4</sup>, triggering an ELM burst that abruptly suppresses both the QCM and pedestal structure. Magnetic fluctuations during ELMs (Figure 2(e)) exhibit high-frequency components but lack the 50 kHz QCM signature, indicating its electrostatic nature. Post L-H transition, the sustained increase in core density and pedestal  $\nabla n_e$  (Figure 2(a,f)) facilitates QCM excitation. This work focuses on QCM dynamics in the ELM-free phase, where the observed  $\nabla n_e$ -frequency anti-correlation implies shear-mediated turbulence regulation prior to ELM onset.

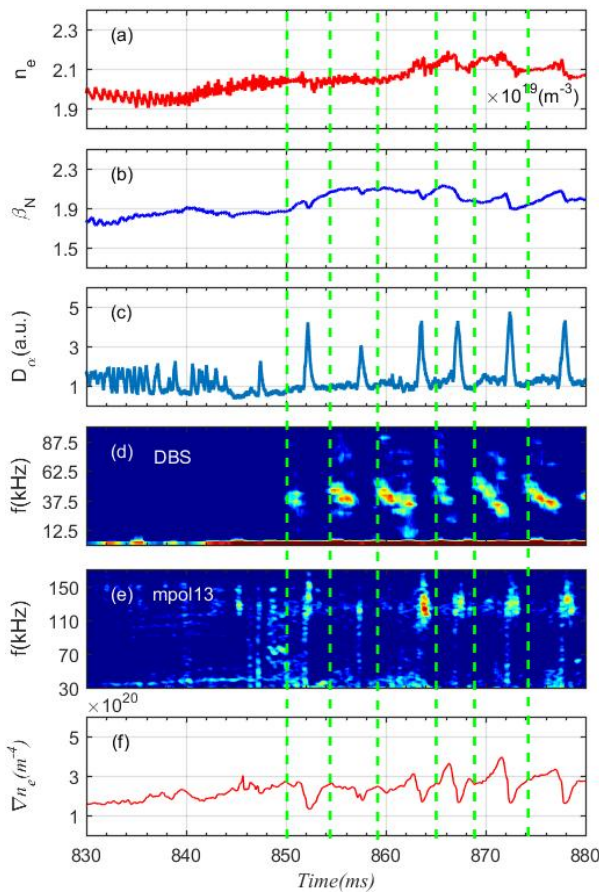


Figure 2. Time evolutions of (a) line averaged density, (b)  $\beta_N$ , (c) divertor  $D\alpha$  emission, spectrograms of (d) ne fluctuations and (e) mirnov coil, (f) density gradient at pedestal.

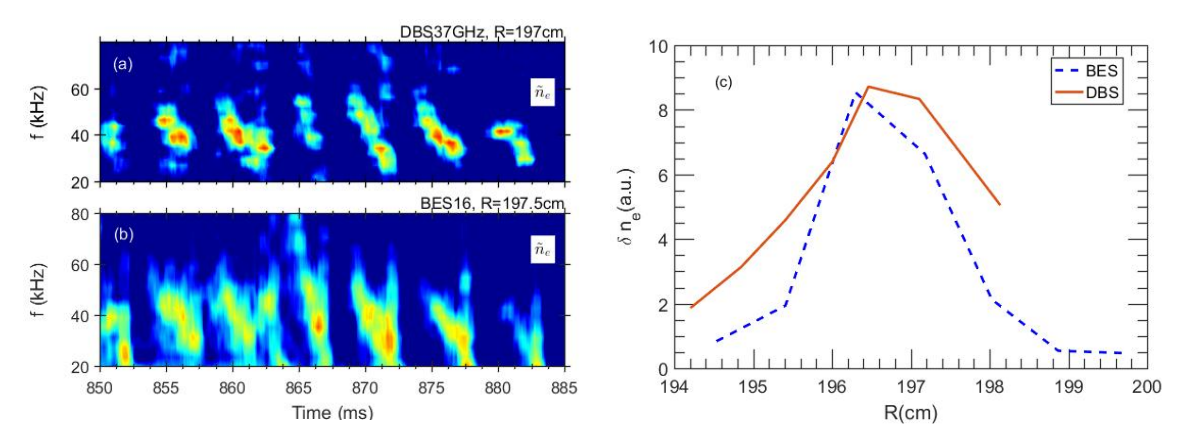


Figure 3. Spectrograms of (a) DBS and (b) BES signals at pedestal, (c) Radial profiles of the density fluctuations of QCM measured by BES and DBS systems.

As shown in figure 1, the 32-channel BES system and 12-channel DBS system deliver both high spatial resolution for precise mode localization and comprehensive coverage across the plasma edge region in both radial and vertical dimensions. Fast Fourier transform (FFT) analysis of density fluctuations from DBS (R = 197 cm) and BES (R = 197.5 cm) measurements, presented in Figures 3(a) and 3(b) respectively, consistently reveals quasicoherent mode (QCM) activity in the 20-60 kHz frequency range. Detailed comparative analysis shows the QCM intensity exhibits a strong radial dependence, decaying with increasing distance from the pedestal and becoming undetectable beyond  $\Delta R > 10$  cm from the last closed flux surface (LCFS). For precise radial localization, we integrate and normalize the 20-60 kHz QCM fluctuations against the total fluctuation amplitude across different radii, with the resulting profile (Figure 3(c)) demonstrating peak amplitude at R ~ 197 cm, precisely coinciding with the steepest gradient region ( $\nabla n_e > 2 \times 10^{20} \text{ m}^{-4}$ ) of the pedestal as confirmed by simultaneous frequency-modulated continuous wave (FMCW) reflectometer measurements. This multi-diagnostic analysis conclusively establishes the OCM as a pedestal-localized mode, with its spatial distribution tightly constrained to the narrow region (196-198 cm) where both the density gradient and electric field shear satisfy theoretical stability conditions for drift-wave-type instabilities.

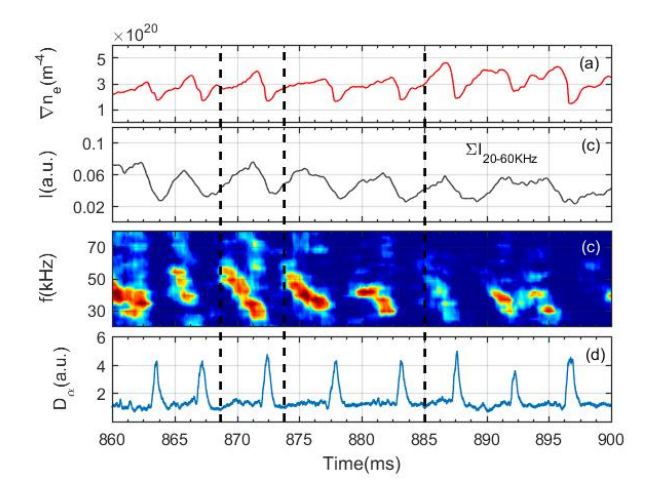


Figure 4. Time evolutions of (a) density gradient at pedestal, (b) density fluctuation amplitude (f=20-60 kHz), (c) spectrogram of DBS signal and (d) divertor Dα emission.

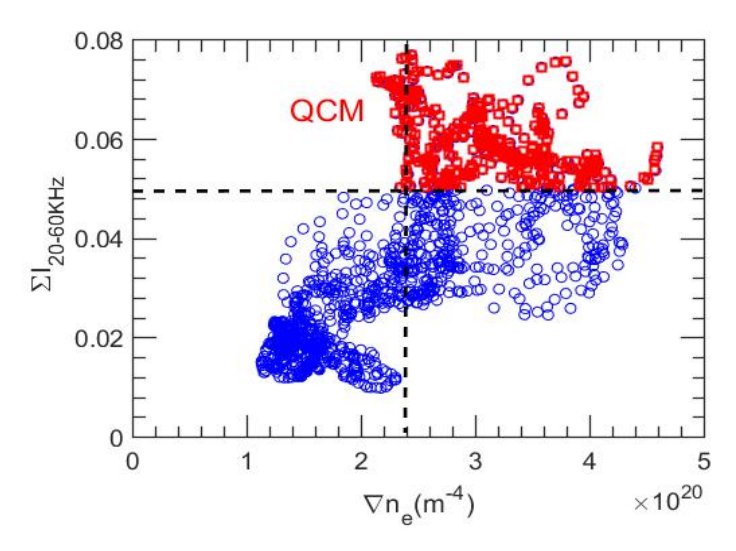


Figure 5. Dependence of density fluctuation amplitude between 20-60 kHz on the density gradient at pedestal. The red squares denote existence of QCMs.

When the density gradient exceeds the critical threshold, the excitation probability of the quasi-coherent mode (QCM) increases significantly. Experimental observations in Figure 3 demonstrate that as the density gradient ( $\nabla$ ne) in the pedestal region continues to rise, the amplitude and frequency of QCM exhibit distinct dynamic response characteristics. Statistical analysis of 16 recurring QCM events (see Figure 4) reveals that during the initial excitation phase, the amplitude can reach 2-4 times that of the background turbulence, with characteristic frequencies typically ranging between 20-60 kHz. However, when  $\nabla$ ne further increases beyond  $4\times10^{\circ}20$  m $^{\circ}$ -4, the QCM amplitude decays at a rate of approximately 20% per  $10^{\circ}20$  m $^{\circ}$ -4, while the characteristic frequency decreases at a gradient of about 10 kHz/( $10^{\circ}20$  m $^{\circ}$ -4)/ms.

This nonlinear response suggests the existence of two competing mechanisms: on one hand, the critical gradient threshold is a necessary condition for QCM excitation; on the other hand, an excessively high density gradient ( $\nabla$ ne > 4×10<sup>20</sup> m<sup>4</sup>) enhances radial electric field shear, suppressing the development of turbulent structures through the E×B flow shear effect. This phenomenon aligns with previous simulation results, indicating that QCM excitation exhibits an optimal gradient window, which holds significant implications for understanding the balance between boundary plasma transport and confinement.

## 4. Effects of QCM on the dynamics of pedestal turbulence

Quasi-Coherent Modes (QCMs), observed primarily in density fluctuations with central frequencies ranging from 20 kHz to 60 kHz, are indicative of electrostatic origin. Their excitation coincides with the saturation of the pedestal density gradient, leading to increased profile stiffness sustained until an ELM burst occurs. The presence of QCMs is also associated with an outward shift of the pedestal location and an overall elevation in the average electron density across the pedestal region.

Analysis reveals that these modes rotate in the electron diamagnetic drift direction while propagating radially outward. Their typical averaged poloidal and radial wavenumbers are estimated to be around  $k_{\theta} \sim 1.3~cm^{-1}$  and  $k_r \sim -0.3~cm^{-1}$ , respectively. Furthermore, measurements of ambient turbulence using BES density fluctuations show that the radial and poloidal correlation lengths increase significantly in discharges with QCMs—reaching approximately  $L_{cr} \sim 2.8~cm$  and  $L_{c\theta} \sim 2.5~cm$ , respectively. These values are about 1–2

times larger than those in H-mode plasmas without QCMs, underscoring the role of QCMs in enhancing turbulent transport within the pedestal.[28]

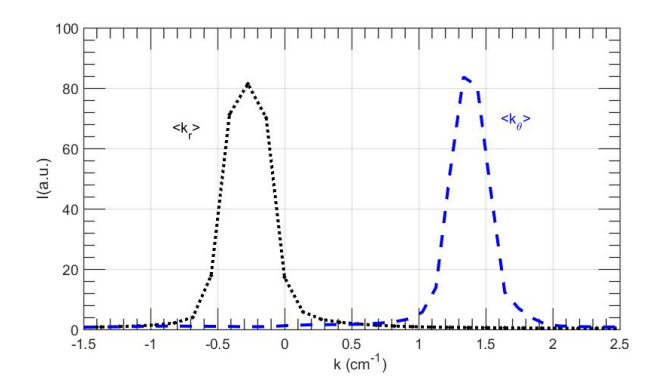


Figure 6: the summed radial and poloidal wavenumber-frequency spectra S(k,f) of the QCMs calculated by the density fluctuations from BES signals.

A strong nonlinear coupling between QCMs and background turbulence has been identified. The QCMs exert both amplitude and phase modulation on the ambient fluctuations, as corroborated by cross-correlation analyses between the turbulence energy and the radial electric field fluctuations of the QCMs. The latter leads the former by several microseconds, confirming a causal relationship.

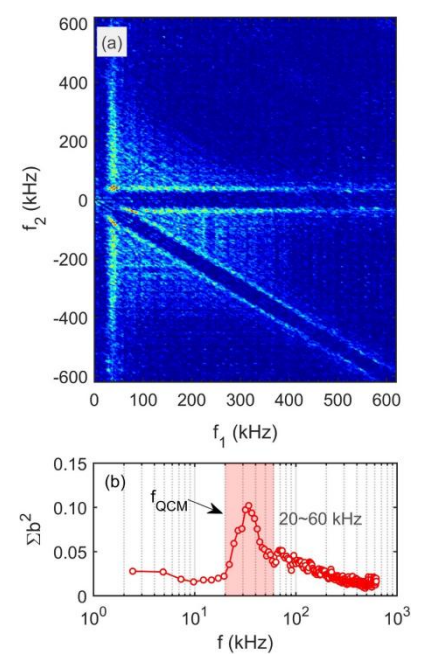


Figure 7: (a) Contour plot of squared autobicoherence of density fluctuations and (b) the corresponding summed squared bicoherence. A significant amplitude of  $\Sigma b^2$  is observed at the QCM frequency ranging , which confirms the presence of substantial nonlinear coupling between QCMs and AT.

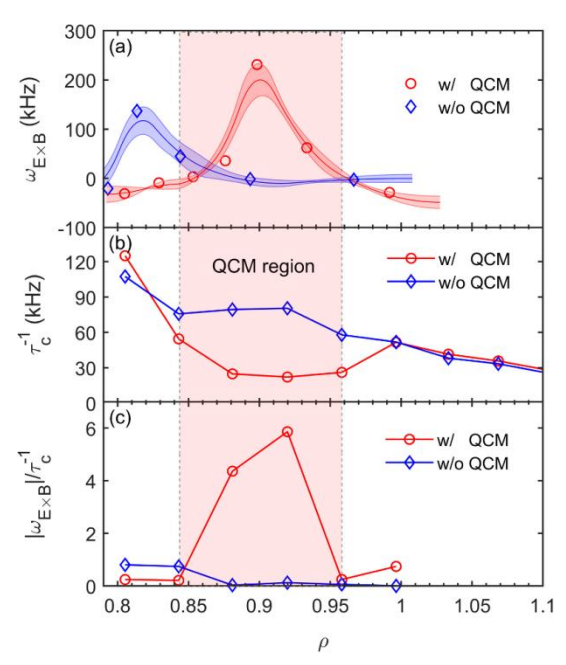


Figure 8: Comparison of turbulence and flow with and without QCM. (a) Flow shearing rate  $\omega_{E\times B}$  calculated from DBS, (b) turbulent decorrelation rate  $\tau_c^{-1}$  from BES measurements and (c) their ratio  $|\omega_{E\times B}|/\tau_c^{-1}$ . The location of QCM is denoted by the shadow region.

Notably, although the turbulence correlation time increases at the QCM location, the flow shearing rate is enhanced sufficiently to suppress turbulent transport. This mechanism supports continued pedestal pressure buildup until the critical gradient for ELM instability is reached. These results highlight the essential role of QCMs in regulating pedestal turbulence dynamics and reinforcing pedestal stability, which may provide key insights for optimizing tokamak performance and controlling ELM bursts.

### 5. Summary and discussion

In summary, the observed QCMs are localized in the pedestal region and are related to the saturation of density gradient in the pedestal. Nonlinear couplings between QCMs and ambient turbulence have been observed and also verified through the envelope modulation of turbulence in density by the radial electrical field fluctuation of the modes. The presence of QCMs can increase the radial and poloidal turbulence correlation lengths, thereby modulating the turbulent transport. Experimental results show that QCMs significantly impact pedestal turbulence and transport by increasing the correlation length as well as the decorrelation time of turbulent eddies. The flow shearing rate in pedestal region is also enhanced to a level that surpasses the decorrelation frequency of turbulence, thus, the existence of QCMs has the ability to put off the ELM burst due to relative stronger stabilization of turbulence by sheared flows. The above results have demonstrated that the pedestal dynamics is largely determined by the complex interactions among QCMs, turbulence and the shear flow.

#### **ACKNOWLEDGEMENTS**

This work was supported by the National MCF Energy R&D Program (Grant No.2024YFE03190001), the National Natural Science Foundation of China (Grant No. 12405254 and 12175055), Nuclear Technology R&D Program (Grant No. HJSYF2024(02)), the Innovation Program of Southwestern Institute of Physics (Grant No. 202301XWCX001), and the Science and Technology Plan Project in Sichuan Province of China (Grant No. 2023ZYD0014). It is also partially supported within the framework of the cooperation between the French Commissariat l'Energie Atomique et aux Energies Alternatives (CEA) and the China National Nuclear Corporation (CNNC).

#### REFERENCES

- [1] W.H. Lin et al., Nucl. Fusion 63(2023) 126048
- [2] P.W. Shi et al., Nucl. Fusion 61 (2021) 096025
- [3] Kamiya K. et al Plasma Phys. Control. Fusion 49(2007) S43
- [4] X.Q. Ji et al., Scientific Reports 6, 32697(2016)
- [5] W.Horton et al., Rev. Mod. Phys. 71(1999)735
- [6] D.L. Yu et al., Nucl. Fusion 56(2016)056003
- [7] J.Wen et al., Phys. Plasmas 30 (2023)112502
- [8] M. Jiang, et al., Nucl. Fusion 62 (2022) 076025
- [9] J. Kalis et a., Nucl. Fusion 64(2024)016038
- [10] Woochang Lee et al., Nucl. Fusion 61(2021)016008
- [11] W.L. Zhong et al., Physics of Plasmas 23, (2016) 060702
- [12] K. J. Zhao, et al., Phys. Rev. Lett. 96, (2006)255004
- [13] H.Wang et al., Phys. Rev. Lett. 112 (2014) 185004
- [14] H.Arnichand et al., Nucl. Fusion 55 (2015) 093021
- [15] A. Diallo et al., Phys. Rev. Lett. 112 (2014) 115001
- [16] S.Banerjee et al., Phys. Plasmas 23 (2016) 044502
- [17]Y.Shen et al., Nucl. Fusion 59 (2019) 044001
- [18] W.Lee et al., Nucl. Fusion 61 (2020)016008
- [19] Larakers J.L et al., Phys. Rev. Lett. 126 (2021)225001
- [20] Curie M.T. et al., Phys. Plasmas 29 (2022 )042503
- [21 Bowman C. et al., Nucl. Fusion 58 (2017) 016021

- [22] Hatch D. et al., Nucl. Fusion 61 (2021)036015
- [23] Yan Z., et al., Phys. Rev. Lett. 107 (2011)055004
- [24] Laggner F.M. et al., Plasma Phys. Control. Fusion 58 (2016)065005
- [25] Diallo A., et al., Phys. Rev. Lett. 121 (2018)235001
- [26] Jiang M. et al., Nucl. Fusion 60 (2020)066006
- [27] Cheng J. et al., Nucl. Fusion 60 (2020)086014
- [28] J. Wen, et al., Nucl. Fusion 64 (2024) 076054
- [29] Xu X.Q., et al., Phys. Plasmas 7 (2000)1951
- [30] Z.C.Yang et al., Phys. Plasmas 23, (2016) 012515
- [31] Biglari H., et al., Phys. Fluids B 2 (1990)1
- [32] Duan X. et al Nucl. Fusion 57 (2017)102013
- [33] Z.B.Shi et al., Plasma Sci. Technol. 20 (2018) 094007
- [34] Z.B.Shi et al., Rev. Sci. Instrum. 89, (2018)10H104
- [35]Ke R. et al Rev. Sci. Instrum. 89 (2018) 10D122